A stabilized DG-type method for solving efficiently Helmholtz problems

Mohamed Amara, Henri Calandra, Rabia Djellouli, Magdalena Grigoroscuta-Strugaru

A stabilized DG-type method for solving efficiently Helmholtz problems

Mohamed Amara — Henri Calandra — Rabia Djellouli —

Magdalena Grigoroscuta-Strugaru

N° 7461

November 2010

*R*apport
de recherche

A stabilized DG-type method for solving efficiently Helmholtz problems

Mohamed Amara* , Henri Calandra[†] , Rabia Djellouli[‡],
Magdalena Grigoroscuta-Strugaru[§]

Abstract: We propose a stabilized discontinuous Galerkin-type method (SDGM) for solving efficiently Helmholtz problems. This mixed-hybrid formulation is a two-step procedure. Step 1 consists in solving well-posed problems at the element partition level of the computational domain, whereas Step 2 requires the solution of a global system whose unknowns are the Lagrange multipliers. The main features of SDGM include: (a) the resulting local problems are associated with *small positive definite* Hermitian matrices that can be solved in parallel, and (b) the matrix corresponding to the global linear system arising in Step 2 is Hermitian and *positive semi-definite*. Illustrative numerical results for two-dimensional waveguide problems highlight the potential of SDGM for solving efficiently Helmholtz problems in mid- and high-frequency regime.

Key-words: Helmholtz equation, discontinuous Galerkin, plane waves, Lagrange multipliers, positive semi-definite Hermitian matrix, inf-sup condition, stability, waveguide problems

* INRIA Bordeaux Sud-Ouest Research Center, Team Project Magique-3D and LMA/CNRS UMR 5142, Université de Pau et des Pays de l'Adour, France
e-mail: mohamed.amara@univ-pau.fr
[†] TOTAL, Avenue Larribau, Pau, France
e-mail: henri.calandra@total.com
[‡] IRIS - Interdisciplinary Research Institute for the Sciences, California State University Northridge and INRIA Bordeaux Sud-Ouest Research Center, Associate Team Project MAGIC, USA
e-mail: rabia.djellouli@csun.edu
[§] BCAM - Basque Center for Applied Mathematics, Bilbao, Spain and INRIA Bordeaux Sud-Ouest Research Center, Team Project Magique-3D, Université de Pau et des Pays de l'Adour, France
e-mail: magdalena.grigoroscuta@univ-pau.fr

Une méthode stabilisée de type DG pour la résolution de problèmes de Helmholtz

Résumé : Nous proposons une méthode stabilisée de type Galerkin discontinu (SDGM) pour la résolution de problèmes de Helmholtz. Cette formulation mixte duale est une procédure en deux étapes. La première étape consiste à résoudre des problèmes bien posés au niveau des éléments du maillage. Dans la deuxième étape nous résolvons un système global dont les inconnues sont les multiplicateurs de Lagrange. Les propriétés principales de SDGM incluent: (a) les systèmes linéaires locaux sont Hermitiens, définis positifs et de petite taille; ils peuvent donc être résolus en parallèle et (b) la matrice du système linéaire global obtenu à l'étape 2 est Hermitienne et semi-définie positive. Nous présentons des résultats numériques pour des problèmes de guide d'ondes 2D qui montrent le potentiel de SDGM pour résoudre efficacement les problèmes de Helmholtz en régime moyenne et haute fréquence.

Mots-clés : équation de Helmholtz, Galerkin discontinu, ondes planes, multiplicateurs de Lagrange, matrice Hermitienne semi-définie positive, condition inf-sup, stabilité, guide d'ondes

1 Introduction

The wave propagation is a physical phenomenon with important applications in various domains such as medical imaging, radar and sonar detection, exploration seismology, non-destructive testing. The mathematical models associated to these physical processes are well understood from a mathematical view point. However, the computation of the solutions is still a challenging problem in spite the tremendous effort dedicated by applied mathematicians and engineers in the last two decades for the development of alternative techniques (see for example, the monograph [16] and the references therein). This difficulty is clearly visible in the case of Helmholtz problems, that describe time-harmonic wave propagation, when computing the solutions for large wavenumber values. Indeed, the standard finite element method (FEM) is not suited for solving Helmholtz problems in the mid- and high-frequency regime because of the quasi-optimality constant which grows with the wavenumber, as explained in details in [4]. Increasing the number of elements in the mesh and/or the order of the element in order to reach an acceptable level of accuracy leads to a prohibitive computational cost for high wavenumbers. For example, it has been reported in [22] that solving an acoustic scattering problem using quadratic finite elements for $ka = 10$, where k is the wavenumber and a characterizes the dimension of the considered submarine-like scatterer, requires solving a system with about 10 million complex unknowns, whereas sonar applications require solving this class of exterior Helmholtz problems for ka larger than 200.

Reducing the computational cost while maintaining a satisfactory level of accuracy has been the motivation of the alternative techniques designed in the last decades for solving Helmholtz problems. Among these emerging methods, one can distinguish those that incorporate the plane waves as shape functions, since these functions are expected to better approximate highly oscillating functions. Examples of such methods include the weak element method for Helmholtz equation [18], the partition of unity method [3], the ultra-weak variational method [5], the least-squares method (LSM) [17], the Trefftz-type wave-based method [6, 10] and the discontinuous Galerkin method (DGM) designed by Farhat *et al* [7, 8, 9]. The latter method appears to be very promising since it is simple to understand and implement, and, more importantly, very efficient when compared to the standard Galerkin FEM. For example, for $ka \geq 10$ and for a level of accuracy of 10% on the relative error, the so-called R-4-1 element reduces the total number of degrees of freedom (dofs) required by the $Q1$ finite element by - at least - a factor five. Similar results are obtained for higher-order elements such as the R-8-2 element which requires 7.2 times less dofs than the $Q2$-based discretization for a 1% prescribed relative error. In spite of this impressive performance, the DGM formulation exhibits numerical instabilities when refining the mesh, that can deteriorate significantly the accuracy of the solution (more than two orders of magnitude), as illustrated in Section 5 and also in [1, 11]. Such instabilities are mainly due to the fact that the elementary matrices become nearly singular while refining the mesh, which makes the system severely ill-conditioned.

We propose a DG-type method, called SDGM (Stabilized Discontinuous Galerkin Method), for the solution of mid- to high-frequency Helmholtz problems. The

method can be viewed as being "between" the DGM formulation designed by
Farhat *et al* [7, 8, 9] and the LSM formulation designed by Monk-Wang [17].
The new proposed solution methodology distinguishes itself from existing proce-
dures by the well-posed character of the local problems, associated to Hermitian
positive definite matrices, and by the resulting global system, which is associ-
ated to a Hermitian positive semi-definite matrix. More specifically, SDGM is
based on a decomposition of the domain in quadrilateral- or triangular-shaped
elements. The solution is approximated, at the element level, by a superposition
of plane waves that are solution of the Helmholtz equation. The continuity of
the solution at the interior interfaces of the elements is then enforced by La-
grange multipliers. Unlike DGM, the proposed method does not preserve the
continuity of the normal derivative. Consequently, Lagrange multipliers are in-
troduced to restore the continuity in the least-squares sense for the traces of
the field and its normal derivative across the interior boundaries of the mesh.
Such choice leads to solving (a) local boundary value problems that are well
posed in the sense of Hadamard and (b) a global system whose unknowns are
the Lagrange multipliers. Note that this system is different from the one arising
in LSM. Indeed, in the LSM formulation the unknown is the field defined in the
interior of the elements. As a consequence, the linear systems obtained at the
discrete level in the two methods have different sizes, as explained in detail in
Section 4. Observe that the proposed technique is a two-step procedure. We first
solve linear systems with positive definite matrices corresponding to the local
problems, and then the Lagrange multipliers are evaluated by solving a linear
system with positive semi-definite matrix. This two-step approach allows us to
consider equally structured and unstructured meshes with either triangular- or
quadrilateral-shaped elements. We must point out that recently we have at-
tempted to modify DGM to restore its stability. The resulting method called
mDGM outperforms DGM, but still remains unstable [1, 11]. SDGM has the
potential to be more robust and stable and therefore to deliver results with a
better level of accuracy while refining the mesh.

The remainder of the paper is organized as follows. In Section 2, we introduce
the model problem and specify the notations. Section 3 is devoted to the pre-
sentation of the continuous and the algebraic formulation of SDGM. In Section
4, we describe the computational complexity of SDGM. Illustrative numerical
results comparing the performance of SDGM to DGM are presented in Section
5. A summary of the salient features of the method, as well as concluding s are
presented in Section 6.

2   Preliminaries

We consider the following class of waveguide-type problems:

$$(\text{BVP}) \begin{cases} -\Delta u - k^2 u & = f & \text{in } \Omega \\ \partial_n u & = \mathrm{i}ku + g & \text{on } \partial\Omega, \end{cases}$$

where $\Omega \subset \mathbb{R}^2$ is an open bounded region with a smooth boundary $\partial\Omega$. k is a
positive number representing the wavenumber. ∂_n is the outward normal deriva-
tive. f and g are complex valued functions in $L^2(\Omega)$ and $L^2(\partial\Omega)$ respectively.
The second equation of BVP is a representation of a class of non-homogeneous

Robin boundary conditions. Other types of boundary condition can be considered as well.

Note that BVP is considered here for its simplicity since it allows us to compute analytically the solution u for a suitable choice of Ω, f and g. An explicit expression of u is crucial for assessing the accuracy of the proposed solution methodology by avoiding the error due to the numerical approximation of u.

In what follows, we consider a regular triangulation τ_h of Ω into quadrilateral- or triangular-shaped subdomains K whose boundaries are denoted by ∂K. The step size mesh discretization is denoted by h. We first introduce the local space defined by:

$$\mathcal{V}(K) = \left\{ v^K \in H^1(K), \, \Delta v^K + k^2 v^K = 0 \text{ in } K \right\}. \tag{1}$$

Next, we define the space of the primal variable to be:

$$\mathcal{V} = \left\{ v \in L^2(\Omega); \, v|_K = v^K \in \mathcal{V}(K) \right\}. \tag{2}$$

Observe that $\mathcal{V}$ contains elements that are discontinuous across interior boundaries since they are only in $L^2(\Omega)$. Therefore, for any $v \in \mathcal{V}$, we define the jump across an interior edge $e = \partial K \cap \partial K'$ of two elements K and K' by:

$$[v] = v^K - v^{K'}.$$

Last, the space of the dual variable corresponding to the Lagrange multipliers, is:

$$\mathcal{M} = \left\{ \mu \in \prod_{K \in \tau_h} L^2(\partial K); \, \mu^K = 0 \text{ on } \partial K \cap \partial \Omega \right\},$$

where μ^K designates the restriction of μ to ∂K: $\mu^K = \mu|_{\partial K}$. For any function $\mu \in \mathcal{M}$, we define the jump across an interior edge $e = \partial K \cap \partial K'$ by:

$$[[\mu]] = \mu^K + \mu^{K'}.$$

3 The proposed solution methodology

3.1 The continuous formulation

The basic idea of SDGM is to evaluate u the solution of BVP using the following splitting:

$$u = \Phi(\lambda) + \varphi, \tag{3}$$

where φ and Φ are in of $\mathcal{V}$ and λ is in $\mathcal{M}$. These quantities are determined through the following two steps:

Step 1 We compute φ and $\Phi(\mu)$, for all $\mu \in \mathcal{M}$. This is achieved by solving a set of local Helmholtz problems. This step is called the *restriction procedure*.

Step 2 We determine $\lambda \in \mathcal{M}$ by solving a global linear system that restores the continuity in the least-squares sense of u given by (3) and its normal derivative, that is:

$$\lambda = \arg \min_{\mu \in \mathcal{M}} \sum_{e-\mathrm{interior\ edge}} \left(\| [\varphi + \Phi(\mu)] \|_{0,e}^2 + \| [[\partial_n \varphi + \partial_n \Phi(\mu)]] \|_{0,e}^2 \right). \quad (4)$$

This step is called the *optimization procedure.*

3.1.1   The restriction procedure

This step is devoted to the computation of φ and $\Phi(\mu)$, for all $\mu \in \mathcal{M}$. It is achieved by solving local Helmholtz problems. More specifically, for all $K \in \tau_h$ and for all $\mu \in \mathcal{V}$, we determine φ^K and $\Phi(\mu^K)$ by solving the following boundary value problems:

$$(\mathrm{BVP1}) \begin{cases} \mathrm{Find}\ \varphi^K \in \mathcal{V}(K)\ \mathrm{such\ that:} \\ \quad -\Delta\varphi^K - k^2\varphi^K \ = \ f & \mathrm{in}\ K \\ \quad \partial_n \varphi^K \ = \ \mathrm{i}k\varphi^K + g & \mathrm{on}\ \partial K \cap \partial\Omega \\ \quad \partial_n \varphi^K \ = \ \mathrm{i}\alpha\varphi^K & \mathrm{on}\ \partial K \cap \Omega, \end{cases}$$

and

$$(\mathrm{BVP2}) \begin{cases} \mathrm{Find}\ \Phi\left(\mu^K\right) \in \mathcal{V}(K)\ \mathrm{such\ that:} \\ \quad -\Delta\Phi\left(\mu^K\right) - k^2\Phi\left(\mu^K\right) \ = \ 0 & \mathrm{in}\ K \\ \quad \partial_n \Phi\left(\mu^K\right) \ = \ \mathrm{i}k\Phi\left(\mu^K\right) & \mathrm{on}\ \partial K \cap \partial\Omega \\ \quad \partial_n \Phi\left(\mu^K\right) \ = \ \mathrm{i}\alpha\Phi\left(\mu^K\right) + \mu^K & \mathrm{on}\ \partial K \cap \Omega. \end{cases}$$

The following observations are noteworthy:

- The presence of $\alpha \in \mathbb{R}_+^*$ ensures the uniqueness of the solution of BVP1 and BVP2, as established in [1] and [11]. At the algebraic level, this term preserves the invertibility of the obtained matrices. This is not the case for DGM, where such term is not present, and therefore the local matrices become nearly singular, as we refine the mesh, due to the fact that k^2 may be close to an interior eigenvalue of the Laplace operator [1, 11]. Note that for all numerical results presented in this paper, we have set $\alpha = k$.

- The regularity of f and g and the standard regularity results for Laplace's operator [12] guarantee that both $\partial_n \varphi^K$ and $\partial_n \Phi\left(\mu^K\right)$ are in $L^2(\partial K)$, for all $\mu \in \mathcal{M}$ (see for example, Theorem 1. and Remark 1. p. 1044 in [2]).

Next, we express the variational formulation of BVP1 and BVP2 in the following compact form:

$$\begin{cases} \mathrm{Find}\ \Psi^K \in \mathcal{V}(K)\ \mathrm{such\ that:} \\ a_K\left(\Psi^K, v^K\right) = l_K\left(v^K\right) & \forall v^K \in \mathcal{V}(K), \end{cases} \quad (5)$$

where $a_K(\cdot, \cdot)$ is a bilinear form defined by:

$$a_K\left(v^K, w^K\right) = \int_{\partial K} \left(\partial_n v^K - \mathrm{i}\,kv^K\right)\overline{(\partial_n w^K - \mathrm{i}\,kw^K)}ds \quad \forall v^K, w^K \in \mathcal{V}(K), \quad (6)$$

and $l_K(\cdot)$ is a linear functional whose expression depends on the considered boundary value problem. In the case of BVP1, $l_K(\cdot)$ is given by:

$$
\begin{aligned}
l_K\left(v^K\right) = {} & \int_{\partial K \cap \partial \Omega} \left(g^K - \frac{\mathrm{i}}{k|K|} \int_K f \, dx \right) \overline{(\partial_n v^K - \mathrm{i}\, k v^K)} ds \\
& - \frac{\mathrm{i}}{k|K|} \int_K f \, dx \int_{\partial K \cap \mathring{\Omega}} \overline{(\partial_n v^K - \mathrm{i}\, k v^K)} ds,
\end{aligned}
\tag{7}
$$

whereas in the case of BVP2, $l_K(\cdot)$ satisfies:

$$
l_K\left(v^K\right) = \int_{\partial K \cap \mathring{\Omega}} \mu^K \overline{(\partial_n v^K - \mathrm{i}\, k v^K)} ds.
\tag{8}
$$

The following result, that can be easily established (see [1, 11]), states the equivalence between BVP1 and BVP2 and the variational problems given by Eqs. (5),(7) and (5),(8) respectively.

Lemma 1
(i) Ψ^K is solution of the variational problem (5), (8) if and only if Ψ^K is solution of BVP2.
(ii) Assume f to be constant on K for all $K \in \tau_h$. Then, Ψ^K is solution of the variational problem (5), (7) if and only if $\Psi^K - \dfrac{1}{k^2} f^K$ is solution of BVP1.

Remark 1 Note that f is constant at the element level for most applications. In fact, $f = 0$ for acoustic scattering problems. Therefore, and for the simplicity of the presentation, we assume from now on that $f = 0$.

Observe that the bilinear form $a_K(\cdot, \cdot)$ given by Eq. (6) is Hermitian. Moreover, using Green's formula, one can easily obtain:

Lemma 2 The bilinear form $a_K(\cdot, \cdot)$ given by Eq. (6) can be expressed as follows:

$$
a_K\left(v^K, w^K\right) = \int_{\partial K} \left(\partial_n v^K \partial_n \overline{w^K} + k^2 v^K \overline{w^K} \right) ds,
\tag{9}
$$

and therefore, $a_K(\cdot, \cdot)$ is positive definite.

Remark 2 We must point out that, at the algebraic level, we use the expression of the bilinear form $a_K(\cdot, \cdot)$ given by Eq. (9) rather than the one given by Eq. (6).

To conclude, Step 1 can be viewed, to some extent, as being a prediction step. It delivers $\varphi + \Phi(\mu) \in \mathcal{V}$, where $\varphi|_K = \varphi^K$, solution of BVP1 and $\Phi(\mu)|_K = \Phi\left(\mu^K\right)$, solution of BVP2, for all $\mu \in \mathcal{M}$. At this stage, we still do not have λ such that $\Phi(\lambda)$ is the needed component in Eq. (3).

3.1.2   The optimization procedure

The objective here is to determine $\lambda \in \mathcal{M}$ for which the function $\varphi + \Phi(\lambda)$ is in $H^1(\Omega)$ with continuous normal derivative. This requirement can be viewed as a correction stage since we select here the best-fit Lagrange multiplier λ. The determination of λ is accomplished by minimizing the functional given by Eq. (4), which leads to solving the following global variational problem:

$$\begin{cases} \text{Find } \lambda \in \mathcal{M} \text{ such that} \\ b(\lambda, \mu) = r(\mu), \quad \forall \mu \in \mathcal{M}, \end{cases} \tag{10}$$

where the bilinear form $b(\cdot, \cdot)$ is given by:

$$
\begin{aligned}
b(\eta, \mu) = \quad & \sum_{e\text{-interior edge}} \beta_e \int_e [\Phi(\eta)] \, \overline{[\Phi(\mu)]} ds \\
+ & \sum_{e\text{-interior edge}} \gamma_e \int_e [[\partial_n \Phi(\eta)]] \, \overline{[[\partial_n \Phi(\mu)]]} ds \\
+ & \sum_{e \subset \partial\Omega} \omega_e \int_e (\partial_n \Phi(\eta) - \mathrm{i}\, k \Phi(\eta)) \, \overline{(\partial_n \Phi(\mu) - \mathrm{i}\, k \Phi(\mu))} ds,
\end{aligned}
\tag{11}
$$

and the linear functional $r(\cdot)$ is given by:

$$
\begin{aligned}
r(\mu) = \quad - & \sum_{e\text{-interior edge}} \beta_e \int_e [\varphi] \, \overline{[\Phi(\mu)]} ds \\
- & \sum_{e\text{-interior edge}} \gamma_e \int_e [[\partial_n \varphi]] \, \overline{[[\partial_n \Phi(\mu)]]} ds \\
- & \sum_{e \subset \partial\Omega} \omega_e \int_e (\partial_n \varphi - \mathrm{i}\, k\varphi - g) \, \overline{(\partial_n \Phi(\mu) - \mathrm{i}\, k \Phi(\mu))} ds,
\end{aligned}
\tag{12}
$$

The weight parameters β_e, γ_e and ω_e are positive real numbers. The third integral in Eq. (11) (resp. in Eq. (12)) is theoretically equal to 0 due to the second boundary condition given by BVP2 (resp. BVP1). However, keeping these terms at the algebraic level seems to bring more robustness and stability to the formulation. The variational problem (10)-(12) expresses the continuity in the least-squares sense of the trace of the solution and its normal derivative. The following observations are noteworthy:

- The bilinear form b is Hermitian. Consequently, only half of the corresponding matrix will be stored. Recall that in DGM [7, 8, 9] the global system is symmetric, but not Hermitian.

- At a first glance, it seems that the bilinear form b resembles the one arising in LSM [17]. They are in fact quite different. Indeed, in the resulting variational formulation corresponding to the LSM approach, the unknown is the field to be evaluated at the element level K, whereas in SDGM the unknowns are the Lagrange multipliers defined on the interior boundaries of the domain partition.

The next result states the equivalence between solving BVP and solving the problems arising in the proposed two-step procedure.

Proposition 1
(i) Let $u = \Phi(\lambda) + \varphi$, where for all K, φ^K is the solution of the variational problem (5),(7), and $\Phi\left(\lambda^K\right)$ is the solution of the variational problem (5),(8) with λ being the solution of (10)-(12). Then, u is the unique solution of BVP.
(ii) Conversely, let u be the solution of BVP. For each $K \in \tau_h$, we define λ by:

$$\lambda^K = \left\{ \begin{array}{ll} 0 & \text{on} \quad e \subset \partial K \cap \partial \Omega \\ \partial_n u^K - \mathrm{i}\, k u^K & \text{on} \quad e \subset \partial K \cap \mathring{\Omega}. \end{array} \right. \tag{13}$$

Then, $\lambda \in \mathcal{M}$ is the solution of (10)-(12), with φ being such that $\varphi^K = \varphi|_K$ is the solution of the variational problem (5),(7), and $\Phi(\mu)$ being such that $\Phi(\mu^K) = \Phi(\mu)|_K$ is the solution of the variational problem (5),(8), for all $\mu \in \mathcal{M}$. Moreover, we have $u = \Phi(\lambda) + \varphi$.

Proof of Proposition 1
(i) For all K, let φ^K be the solution of the variational problem (5),(7) and $\Phi\left(\mu^K\right)$ is the solution of the variational problem (5),(8), for all $\mu \in \mathcal{M}$. Then, from Lemma 1 (resp. Lemma 2) we deduce that φ^K (resp. $\Phi\left(\mu^K\right)$) is solution of BVP1 (resp. BVP2).

3.2 The algebraic formulation

The discretization of SDGM requires the introduction of two finite-dimensional subspaces $\mathcal{V}_h$ and $\mathcal{M}_h$ of $\mathcal{V}$ and $\mathcal{M}$ respectively. Hence, $\mathcal{V}_h$ is a space of functions satisfying the Helmholtz equation at the element level K. Examples of such functions include the plane waves [1] and the Bessel functions [17]. We consider only the plane waves in order to compare the performance of SDGM to DGM [7, 8, 9]. The subspace $\mathcal{M}_h$ contains plane waves defined on the interior edges of the domain partition. Note that SDGM allows, in principle, to choose the spaces $\mathcal{V}_h$ and $\mathcal{M}_h$ independently, which is not the case for DGM in which an inf-sup condition must be satisfied. In addition, SDGM does not require the same local space discretization for all the elements in the mesh. Consequently, using an adaptive strategy for both the mesh and the discretization does not increase the implementation complexity in SDGM.
From now on, we denote by $\mathcal{V}_h(K)$ (resp. $\mathcal{M}_h(K)$) the subspace of functions of $\mathcal{V}_h$ (resp. $\mathcal{M}_h$) restricted to K (resp. ∂K). Furthermore, n^K (resp. n^{λ^K}) denotes the dimension of $\mathcal{V}_h(K)$ (resp. $\mathcal{M}_h(K)$). Last, the dimension of $\mathcal{M}_h$, which corresponds to the total number of dofs, is denoted by n^λ.

Next, we show that, when formulated in the finite-dimensional spaces $\mathcal{V}_h$ and $\mathcal{M}_h$, the proposed two-step procedure consists in solving a small linear system which is Hermitian and positive definite (Step 1), and a global Hermitian positive semi-definite system whose unknowns are the Lagrange multipliers (Step 2).

3.2.1 The restriction procedure

Let φ_h and $\Phi_h(\mu_h)$ be the approximations of φ and $\Phi(\mu_h)$ in $\mathcal{V}_h$. It follows from the variational problem (5), (7) (resp. (5), (8)) that φ_h (resp. $\Phi_h(\mu_h)$) is

evaluated by solving in each element K the following linear system:

$$\left(\mathbf{P}^{\partial K} + k^2 \mathbf{S}^{\partial K}\right) \mathbf{x}^K = \mathbf{d}^{\partial K}, \tag{14}$$

where $\mathbf{P}^{\partial K}$ is a stiffness-like matrix defined on ∂K by:

$$\mathbf{P}_{jl}^{\partial K} = \int_{\partial K} \partial_n v_l \partial_n \overline{v_j} ds \quad 1 \le j, l \le n^K, \tag{15}$$

and $\mathbf{S}^{\partial K}$ is a mass-like matrix defined on ∂K by:

$$\mathbf{S}_{jl}^{\partial K} = \int_{\partial K} v_l \overline{v_j} ds \quad 1 \le j, l \le n^K. \tag{16}$$

The vector $\mathbf{x}^K \in \mathbb{C}^{n^K}$ is the coordinate vector of φ_h^K (resp. $\Phi_h\left(\mu_h^K\right)$) in the basis $\{v_l\}_{1 \le l \le n^K}$ for $\mathcal{V}_h^K$. The jth coordinate of $\mathbf{d}^{\partial K}$ is $l_K(v_j)$ given by Eq. (7) (resp. Eq. (8)).

The next result proves that the system is positive definite. This property is crucial for retaining the stability of the computational procedure when refining the mesh partition.

Proposition 2   For any element K of the domain partition, the matrix $\mathbf{B}^K = \mathbf{P}^{\partial K} + k^2 \mathbf{S}^{\partial K}$ of the local system given by Eq. (14) is Hermitian and positive definite.

Proof of Proposition 2   It is clear from Eq. (15) and Eq. (16) that $\mathbf{B}^K$ is a Hermitian matrix. Next, we prove that $\mathbf{B}^K$ is a positive definite matrix.
For any vector $\boldsymbol{z} = {}^t[z_1, z_2, ..., z_{n^K}] \in \mathbb{C}^{n^K}$, we set:

$$\xi_h^K = \sum_{1 \le l \le n^K} z_l v_l^K \in \mathcal{V}_h(K), \tag{17}$$

where $\left\{v_l^K\right\}_{1 \le l \le n^K}$ is the basis for $\mathcal{V}_h(K)$. Then, it follows from Eq. (15) and Eq. (16) that:

$$\boldsymbol{z}^* \mathbf{B}^K \boldsymbol{z} = \|\partial_n \xi_h\|_{L^2(\partial K)}^2 + \|\xi_h\|_{L^2(\partial K)}^2. \tag{18}$$

Consequently, $\boldsymbol{z}^* \mathbf{B}^K \boldsymbol{z} \ge 0$. Next, assume $\boldsymbol{z}^* \mathbf{B}^K \boldsymbol{z} = 0$. Then, it follows from Eq. (18) that:

$$\|\partial_n \xi_h^K\|_{L^2(\partial K)}^2 + \|\xi_h^K\|_{L^2(\partial K)}^2 = 0. \tag{19}$$

Therefore,

$$\partial_n \xi_h^K = 0 \ \text{ on } \partial K \quad \text{and} \quad \xi_h^K = 0 \ \text{ on } \partial K$$

Using the continuation theorem [14, 21], we deduce that $\xi_h^K = 0$ in K. Consequently, $z_l = 0$ for all $1 \le l \le n^K$. Thus, $\boldsymbol{z}^* \mathbf{B}^K \boldsymbol{z} > 0, \forall \boldsymbol{z} \in \mathbb{C}^{n^K} \setminus \{0\}$, that is, $\mathbf{B}^K$ is a positive definite matrix.   ∎

Remark 3

(i) Note that all the entries of the matrix $\mathbf{P}^{\partial K} + k^2 \mathbf{S}^{\partial K}$ can be evaluated analytically when plane wave shape functions are used. In addition, $\mathbf{P}^{\partial K} + k^2 \mathbf{S}^{\partial K}$ is an $n^K \times n^K$ matrix, which is typically a small matrix. Hence, the linear system (14) can be solved by any direct method and in parallel since the problems are independent from an element K to another K'.

(ii) For an element $K \in \tau_h$, solving (14) requires the solution of *only* one $n^K \times n^K$ linear system with $n^{\lambda^K} + 1$ right-hand sides.

3.2.2   The optimization procedure

The variational problem (10)-(12) formulated in the finite dimensional space $\mathcal{M}_h$ leads to the solution of the following global linear system:

$$\mathbf{A}\boldsymbol{y} = \mathbf{f}, \tag{20}$$

where the entries of the matrix $\mathbf{A}$ and the coordinates of the vector $\mathbf{f}$ are given by:

$$
\begin{aligned}
\mathbf{A}_{lm} = & \sum_{e\text{-interior edge}} \beta_e \int_e [\Phi_h(\mu_m)] \,\overline{[\Phi_h(\mu_l)]} ds \\
& + \sum_{e\text{-interior edge}} \gamma_e \int_e [[\partial_n \Phi_h(\mu_m)]]\,\overline{[[\partial_n \Phi_h(\mu_l)]]} ds \\
& + \sum_{e \subset \partial\Omega} \omega_e \int_e (\partial_n \Phi_h(\mu_m) - \mathrm{i}\,k\Phi_h(\mu_m))\,\overline{(\partial_n \Phi_h(\mu_l) - \mathrm{i}\,k\Phi_h(\mu_l))} ds,
\end{aligned}
\tag{21}
$$

and

$$
\begin{aligned}
\mathbf{f}_l \;= & -\sum_{e\text{-interior edge}} \beta_e \int_e [\varphi_h] \,\overline{[\Phi_h(\mu_l)]} ds \\
& - \sum_{e\text{-interior edge}} \gamma_e \int_e [[\partial_n \varphi_h]]\,\overline{[[\partial_n \Phi_h(\mu_l)]]} ds \\
& - \sum_{e \subset \partial\Omega} \omega_e \int_e (\partial_n \varphi_h - \mathrm{i}\,k\varphi_h - g)\,\overline{(\partial_n \Phi_h(\mu_l) - \mathrm{i}\,k\Phi_h(\mu_l))} ds.
\end{aligned}
\tag{22}
$$

The vector $\boldsymbol{y} \in \mathbb{C}^{n^\lambda}$ is the coordinate vector of λ_h in the basis $\{\mu_l\}_{1 \le l \le n^\lambda}$ for $\mathcal{M}_h$. The system is said to be global since the unknowns are defined on all the interior edges of the mesh partition. Note that the matrix $\mathbf{A}$ is Hermitian. In addition, we have:

Proposition 3   The matrix $\mathbf{A}$ is positive semi-definite. Furthermore, if the spaces $\mathcal{V}_h$ and $\mathcal{M}_h$ satisfy the following condition:

$$
\left[\int_{\partial K} \mu_h^K \left(\overline{\partial_n v_h^K - \mathrm{i}\,k v_h^K} \right) ds = 0\,, \quad \forall\, v_h^K \in \mathcal{V}_h(K) \right] \quad \Longrightarrow \quad \mu_h^K = 0\,, \tag{23}
$$

then, the matrix $\mathbf{A}$ is positive definite.

Proof of Proposition 3   For any vector $\boldsymbol{z} = {}^t[z_1, z_2, ..., z_{n^\lambda}] \in \mathbb{C}^{n^\lambda}$, we set:

$$\eta_h = \sum_{1 \leq l \leq n^\lambda} z_l \mu_l. \tag{24}$$

where $\{\mu_j\}_{1 \leq j \leq n^\lambda}$ is a basis for $\mathcal{M}_h$. Then, due to the linearity of BVP2, we have:

$$\Phi_h\left(\eta_h\right) = \sum_{1 \leq l \leq n^\lambda} z_l \Phi_h\left(\mu_l\right). \tag{25}$$

It follows from the expression of the matrix $\mathbf{A}$ (see Eq. (21)) that:

$$\boldsymbol{z}^*\mathbf{A}\boldsymbol{z} = \sum_{e-\text{interior edge}} \left(\beta_e \| \left[\Phi_h\left(\eta_h\right) \right] \|_{L^2(e)}^2 + \gamma_e \| \left[\left[\partial_n \Phi_h\left(\eta_h\right) \right]\right] \|_{L^2(e)}^2 \right)$$
$$+ \sum_{e \subset \partial\Omega} \omega_e \| \partial_n \Phi_h\left(\eta_h\right) - \mathrm{i}\,k\Phi_h\left(\eta_h\right) \|_{L^2(e)}^2. \tag{26}$$

Consequently, $\boldsymbol{z}^*\mathbf{A}\boldsymbol{z} \geq 0$, that is, $\mathbf{A}$ is a positive semi-definite matrix.
Next, we assume that the condition (23) is satisfied. Let $\boldsymbol{z}$ be a vector in $\mathbb{C}^{n^\lambda}$ such that $\boldsymbol{z}^*\mathbf{A}\boldsymbol{z} = 0$. Since $\beta_e > 0$, $\gamma_e > 0$ and $\omega_e > 0$ for any edge e, it follows from Eq. (26) that:

(i) $\left[\Phi_h\left(\eta_h\right) \right] = 0$ on all interior edges e.

(ii) $\left[\left[\partial_n \Phi_h\left(\eta_h\right) \right]\right] = 0$ on all interior edges.

Consequently, we deduce from (i) that $\Phi_h\left(\eta_h\right) \in H^1\left(\Omega\right)$ and therefore, using (ii) and the fact that $\Delta\Phi_h\left(\eta_h^K\right) \in L^2\left(K\right)$ we deduce that $\Delta\Phi_h\left(\eta_h\right) \in L^2\left(\Omega\right)$. Moreover, $\Phi_h\left(\eta_h\right)$ satisfies:

$$\begin{cases} -\Delta\Phi_h\left(\eta_h\right) - k^2\Phi_h\left(\eta_h\right) & = 0 & \text{in } \Omega \\ \partial_n\Phi_h\left(\eta_h\right) & = \mathrm{i}k\Phi_h\left(\eta_h\right) & \text{on } \partial\Omega. \end{cases}$$

This boundary value problem admits a unique solution. Therefore, $\Phi_h\left(\eta_h\right) = 0$ in Ω. Hence, it follows from the discrete form of the variational problem (5)-(8) and the compatibility condition (23) that $\eta_h^K = 0, \forall K \in \tau_h$. Consequently, $\eta_h = 0$. Hence, we deduce from Eq. (24) that $z_l = 0$ for all $1 \leq l \leq n^\lambda$. Thus, $\boldsymbol{z}^*\mathbf{A}\boldsymbol{z} > 0, \forall \boldsymbol{z} \in \mathbb{C}^{n^\lambda} \setminus \{0\}$, that is, $\mathbf{A}$ is a positive definite matrix.   ∎

Remark 4
(i) Observe that condition (23) is a compatibility-type condition between the two discrete spaces, $\mathcal{V}_h$ and $\mathcal{M}_h$. Such condition is verified for example when using eight plane waves for approximating the field in each element and two dofs on each edge of an element for the Lagrange multiplier (which corresponds to the R-8-2 element described in Section 5).
(ii) In all numerical experiments, the system (20) is solved using an LU decomposition method for sparse matrices designed by Pardiso [15, 19, 20].

4   Computation complexity

The computational cost of SDGM depends mainly on the number of shape functions used for the approximation of the Lagrange multipliers. Indeed, the local problems that incur in Step 1 are small linear systems. Their size depends on the number of shape functions that approximate the field, which does not exceed 20 plane waves for all numerical experiments presented in this paper. These systems can be solved efficiently using any direct method. In addition, they can be solved in parallel since the local problems are independent from one element to another. Therefore, the increase in the number of shape functions has a very little effect on the total computational cost, which is not the case for LSM. The cost in SDGM is given mainly by the size and the sparsity pattern of the global matrix given by Eq. (21). More specifically, the number of unknowns of the corresponding system, given by Eq. (20), is the total number of dofs for the Lagrange multiplier, which is also the case for DGM. Note that in both formulations the unknowns of the global system are defined on the interior edges of the mesh partition. However, in SDGM the obtained matrix is Hermitian and positive semi-definite, which allows, in particular, the storage of only half the matrix and the use of robust and efficient existing iterative solvers.

For illustration purpose, consider a square-shaped computational domain to which is applied a rectangular-shaped $n \times n$ mesh, where n designates the number of elements in one direction. Recall that for an element K, n^{λ^K} is the number of dofs for the Lagrange multiplier on the boundary ∂K and n^K is the number of plane waves which approximate the field in K. We report in Table 1 the asymptotic size of the solution vector and the stencil width for the three methods: SDGM, DGM and LSM.

Observe that SDGM has twice as many Lagrange multipliers as DGM. Dou-

Table 1: Asymptotic size of the solution vector and stencil width for a $n \times n$ rectangular-shaped uniform mesh.

Method	Asymptotic size of the solution vector	Stencil width
SDGM	$(4n^{\lambda^K})n^2$	$20n^{\lambda^K}$
DGM	$(2n^{\lambda^K})n^2$	$7n^{\lambda^K}$
LSM	$n^K n^2$	$5n^K$

bling the number of dofs for the Lagrange multiplier is needed to ensure the well-posedness character of the local boundary value problems. It also allows the method to accommodate easily an adaptive-like discretization approach, that is the use of different orders of shape functions for a given mesh. Observe that the stencil in SDGM is three times larger than in DGM. This increase in the computational cost is the price to pay for obtaining a global positive semi-definite matrix in SDGM.

Note that in SDGM approximating the solution locally with different number of plane waves, while introducing the same number of dofs for the Lagrange multiplier, leads to the same size and stencil width of the global matrix. This is not the case in LSM, in which the size and the stencil of the global matrix are directly related to the dimension of the local basis. The computational

cost in LSM is smaller than in SDGM when using lower order elements. How-
ever, LSM is expected to be more expensive when using higher order elements
($n^K > 4n^{\lambda^K}$), which is what is recommended to use to achieve a high level of
accuracy [17]. The computation cost increase may become more important for
three-dimensional problems in the case of high wavenumber values.

5   Performance assessment

We have performed numerical experiments using plane waves shape functions
and we have compared the results to those obtained with DGM. The plane
waves shape functions are:

$$e^{\mathrm{i}\,k(x\,\cos\theta_p + y\,\sin\theta_p)} \quad\text{and}\quad \theta_p = 2(p-1)\pi/n^K \quad 1 \le p \le n^K. \tag{27}$$

n^K is the number of plane waves that approximate the field in the element K.
From now on, we assume Ω to be an $a \times a$ square-shaped domain. We first
compare the two methods when using a uniform mesh partition of Ω. Then, we
analyze the effect of the mesh distortion on the accuracy for both methods. We
measure the level of accuracy using the following modified H^1-norm [7]:

$$\|v\|_{\widehat{H^1}} = \left(\sum_K \|v\|^2_{H^1(K)} + \sum_{e-\mathrm{interior\ edge}} \|[v]\|^2_{L^2(e)} \right)^{\frac{1}{2}}, \quad \forall v \in \mathcal{V}. \tag{28}$$

For all numerical experiments, we have set $\beta_e = k^2$, $\gamma_e = 1$ for the interior edges
and $\omega_e = 1$ for the boundary edges. This choice is motivated by the numerical
experiments we have performed rather than theoretical considerations.

5.1   Uniform mesh

We present two sets of numerical results obtained in the mid-frequency and in
the high-frequency regime respectively.

5.1.1   Low- and mid-frequency regime

First, we consider the case where the exact solution of BVP is a plane wave of
the form:

$$e^{\mathrm{i}\,k(x\,\cos\theta + y\,\sin\theta)}. \tag{29}$$

We evaluate the relative error in the norm given by Eq. (28) for each propa-
gation angle $\theta \in [0, 2\pi)$. We also evaluate the *total* relative error, that is, the
mean value of the relative error obtained when swiping θ over $[0, 2\pi)$.

In the first two experiments, we approximate the solution using eight plane
waves in each element of the mesh ($n^K = 8$). The Lagrange multiplier is then
approximated using successively two dofs:

$$\lambda_h = \mu_1 e^{\mathrm{i}\,k\frac{\sqrt{2}}{4}s} + \mu_2 e^{-\mathrm{i}\,k\frac{\sqrt{2}}{4}s}, \tag{30}$$

and three degrees of freedom:

$$\lambda_h = \mu_1 + \mu_2 e^{\mathrm{i}\, k \frac{\sqrt{2}}{2} s} + \mu_3 e^{-\mathrm{i}\, k \frac{\sqrt{2}}{2} s}. \tag{31}$$

s represents the curvilinear abscissa. These two choices correspond to the so-called R-8-2 and R-8-3 elements respectively [7].

First, we compare the accuracy of the solution delivered by DGM and SDGM for three different values of ka: 10, 20, 30, and for a fixed resolution $kh = \frac{1}{2}$ corresponding to about 12 elements per wavelength. The results reported in Figs. 1-3 reveal the following:

- Fig. 1(a)-(c) demonstrates that enriching the space of approximation for the Lagrange multipliers from two to three dofs per edge in SDGM reduces the relative error with about two orders of magnitude. This is not the case for DGM, as observed in Fig. 1(d)-(f). Indeed, when employing the R-8-3 element in DGM, there is a loss of accuracy of about one order of magnitude when compared to R-8-2. This situation is contrary to what one can expect since three dofs is the full approximation of the Lagrange multipliers in this case. However, this result is not surprising since the discrete inf-sup condition is violated in the case of the R-8-3 element. We must point out that in SDGM we have enriched the discrete space for the Lagrange multipliers up to five dofs per edge, corresponding to the full approximation of the Lagrange multipliers (see [1, 11]), and we have found that the gain in the accuracy compared to R-8-3 is barely noticeable.

- Fig. 2 shows that SDGM equipped with R-8-3 outperforms DGM with R-8-2. Regardless of the values of ka and the propagation angle, the relative error delivered by SDGM is about one order of magnitude smaller than the one obtained with DGM. Note that this superiority is not really important here since the total relative error delivered by each method is less than 1%.

- The analysis of the pollution effect (see Fig. 3) reveals that SDGM exhibits negligible pollution effect. This is also the case for DGM, as already reported in [7, 8, 9].

Next, we analyze the stability of the method to the mesh refinement. The results depicted in Fig. 4 are obtained for $ka = 1$. They clearly demonstrate the superiority in terms of stability of SDGM over DGM. As already observed in [1, 11], DGM is unstable as $kh < \frac{1}{6}$, corresponding to over 36 elements per wavelength, in which case the accuracy level deteriorates dramatically reaching very quickly 100%. On the other hand, the relative error delivered by SDGM remains less than 1% even for a resolution corresponding to over 1000 elements per wavelength! The oscillations observed in the case of SDGM are due to the numerical loss of the linear independence of the basis functions, as indicated in Table 2 and demonstrated theoretically in [11]. Table 2 shows that the smallest eigenvalue for the local system corresponding to SDGM tends to be nearly zero, as we refine the mesh, due to the loss of the linear independence of the shape functions. By removing just one plane wave from the local basis and using the R-7-2 element, we observe a significant improvement in the performance of SDGM, as illustrated below (see Fig. 5 and Table 3). Note that the R-7-2 element introduced in [1], corresponds to $n^K = 7$ in Eq. (27) and the same shape
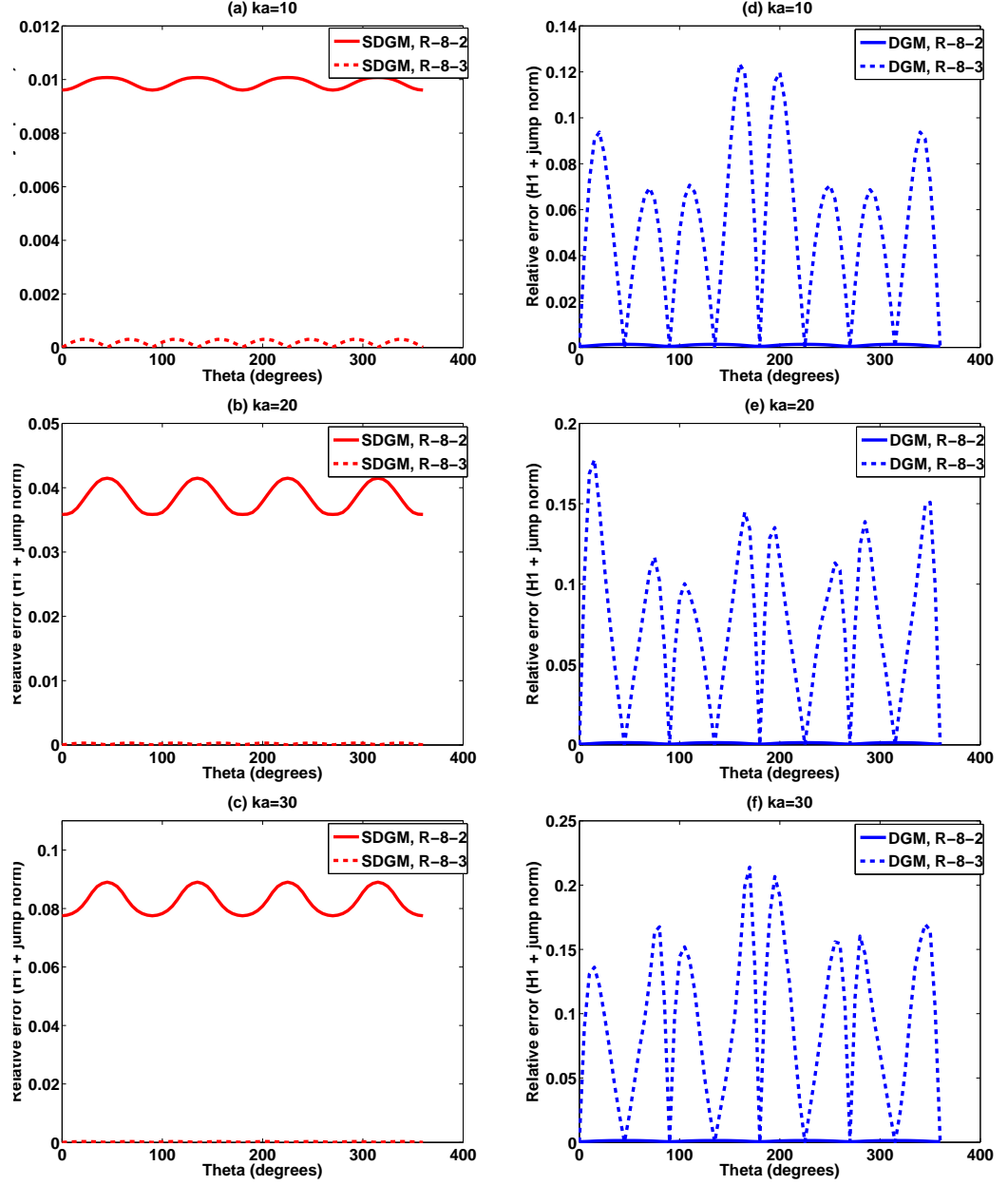
Figure 1: Performance comparison between SDGM (left) and DGM (right) for element R-8-2 and R-8-3, and for a fixed resolution $kh = \frac{1}{2}$.
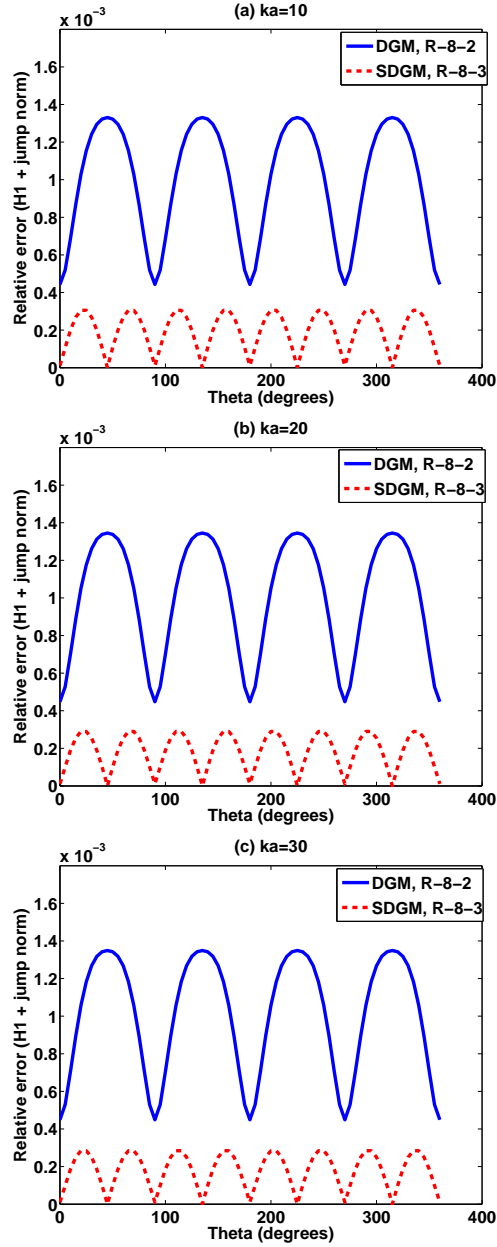
Figure 2: Performance comparison between SDGM equipped with R-8-3 and DGM equipped with R-8-2, for a fixed resolution $kh = \frac{1}{2}$.
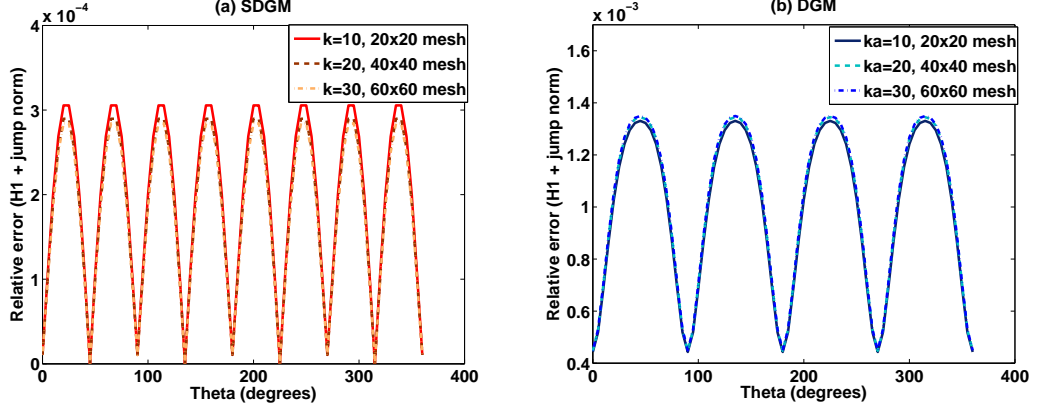
Figure 3: Comparison of the pollution effect: SDGM equipped with R-8-3 (left) and DGM equipped with R-8-2 (right), for a fixed resolution $kh = \frac{1}{2}$.
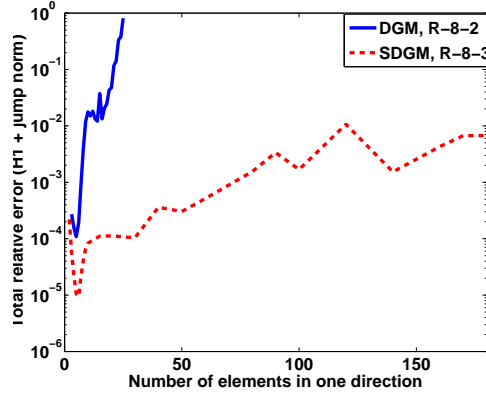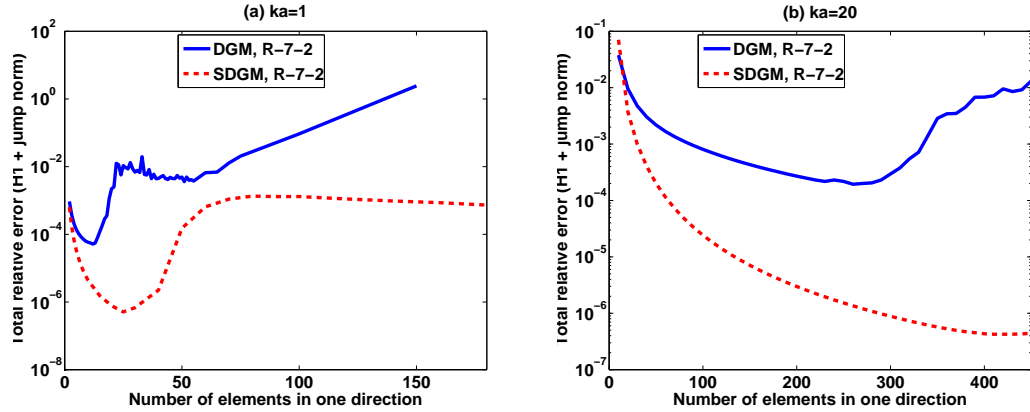

Figure 4: Sensitivity of the total relative error to the mesh refinement: Comparison between SDGM equipped with R-8-3 and DGM equipped with R-8-2, for $ka = 1$.

functions used for R-8-2 to approximate the Lagrange multipliers (see Eq. (30)). We set $ka = 1$ and 20, and we measure the sensitivity of the total relative error with respect to the mesh refinement. The performance of the two methods is depicted in Fig. 5. Table 3 shows the effect of the mesh refinement on the smallest eigenvalue of the local systems for both methods. These two results suggest the following:

- Fig. 5 shows that for both wavenumbers $ka = 1$ and 20, DGM becomes unstable as $kh < \frac{1}{15}$. The accuracy level deteriorates dramatically reaching quickly 100% in the case where $ka = 1$ (see Fig. 5a) and over 20% for $ka = 20$ (see Fig. 5b), whereas SDGM remains very accurate. In SDGM one can notice a loss of accuracy for $ka = 1$ as $h/a < \frac{1}{40}$ (corresponding to over 240 elements per wavelength). Nevertheless, SDGM retains an

Table 2: Dependence with respect to the mesh size of the total relative error and smallest eigenvalue of the local matrices in SDGM and DGM equipped with R-8-2 element, and for $ka = 1$.

	SDGM		DGM	
h/a	Total relative error	The smallest eigenvalue	Total relative error	The smallest eigenvalue
1/5	0.001%	$2.2 \cdot 10^{-09}$	0.01%	$9.5 \cdot 10^{-11} - 4.1 \cdot 10^{-12}\mathrm{i}$
1/10	0.009%	$1.7 \cdot 10^{-11}$	1.8%	$3.7 \cdot 10^{-13} - 7.9 \cdot 10^{-15}\mathrm{i}$
1/15	0.018%	$1.0 \cdot 10^{-12}$	3.8%	$1.5 \cdot 10^{-14} - 2.4 \cdot 10^{-16}\mathrm{i}$
1/20	0.016%	$1.4 \cdot 10^{-13}$	4.7%	$1.5 \cdot 10^{-15} + 5.9 \cdot 10^{-17}\mathrm{i}$
1/25	0.019%	$2.8 \cdot 10^{-14}$	81%	$2.4 \cdot 10^{-16} + 4.4 \cdot 10^{-17}\mathrm{i}$
1/40	0.048%	$1.0 \cdot 10^{-15}$	over 100%	$1.1 \cdot 10^{-17} + 1.6 \cdot 10^{-17}\mathrm{i}$
1/50	0.015%	$1.7 \cdot 10^{-16}$	over 100%	$4.6 \cdot 10^{-18} + 6.3 \cdot 10^{-18}\mathrm{i}$
1/70	0.049%	$1.3 \cdot 10^{-17}$	over 100%	$-3.5 \cdot 10^{-19} + 1.9 \cdot 10^{-18}\mathrm{i}$
1/100	0.140%	$-4.2 \cdot 10^{-17}$	over 100%	$3.6 \cdot 10^{-19} + 4.4 \cdot 10^{-17}\mathrm{i}$

Figure 5: Sensitivity of the total relative error to the mesh refinement: Comparison between SDGM and DGM equipped with R-7-2, for $ka = 1$ (left) and $ka = 20$ (right).

acceptable level of accuracy (less than 0.1%) even for a resolution corresponding to over 1200 elements per wavelength!

- A quick comparison between Table 2 and Table 3 shows that removing one plane wave from the local basis makes the decay of the smallest eigenvalue significantly slower. There is a difference of about four orders of magnitude. Nevertheless, DGM remains unstable, as expected, due to the ill-posedness character of the formulation at the element level.

Next, we analyze the performance of SDGM when equipped with higher-order elements. More specifically, we enrich the local basis by taking eleven shape

Table 3: Dependence with respect to the mesh size of
the total relative error and smallest eigenvalue of the
local matrices in SDGM and DGM equipped with R-
7-2, and for $ka = 1$.

h/a	SDGM		DGM	
	Total relative error	The smallest eigenvalue	Total relative error	The smallest eigenvalue
1/5	0.003%	$3.1 \cdot 10^{-06}$	0.01%	$1.4 \cdot 10^{-07} - 6.6 \cdot 10^{-09}$i
1/10	0.0004%	$9.7 \cdot 10^{-08}$	0.006%	$2.1 \cdot 10^{-09} - 5.2 \cdot 10^{-11}$i
1/15	0.0001%	$1.3 \cdot 10^{-08}$	0.01%	$1.8 \cdot 10^{-10} - 3.0 \cdot 10^{-12}$i
1/20	0.00007%	$3.0 \cdot 10^{-09}$	0.02%	$2.5 \cdot 10^{-11} - 4.1 \cdot 10^{-13}$i
1/25	0.00005%	$1.0 \cdot 10^{-09}$	1%	$8.7 \cdot 10^{-12} - 8.5 \cdot 10^{-14}$i
1/40	0.0002%	$9.5 \cdot 10^{-11}$	0.4%	$5.2 \cdot 10^{-13} - 3.1 \cdot 10^{-15}$i
1/50	0.015%	$3.1 \cdot 10^{-11}$	0.5%	$1.4 \cdot 10^{-13} - 6.7 \cdot 10^{-16}$i
1/70	0.1%	$5.8 \cdot 10^{-12}$	1.2%	$1.8 \cdot 10^{-14} - 5.7 \cdot 10^{-17}$i
1/100	0.1%	$9.7 \cdot 10^{-13}$	10%	$2.1 \cdot 10^{-15} + 2.4 \cdot 10^{-18}$i

functions in each element K ($n^K = 11$ in Eq. (27)) and the three basis functions used in R-8-3 for the approximation of the Lagrange multipliers (see Eq. (31)). This element is called R-11-3 [1, 11]. We set $ka = 20$ and we evaluate the total relative error obtained while refining the mesh. We compare the results to the ones obtained when SDGM is equipped with R-7-2. These results are reported in Table 4. They show that for a fixed resolution, R-11-3 improves the accuracy over R-7-2 with more than two orders of magnitude. Note that this significant gain is obtained by increasing the computational cost by about 50% only (see Table 4). These results clearly suggest that it is preferable to use higher-order elements rather than refining the mesh to improve the accuracy.

On the other hand, we have observed in [11] that SDGM and LSM exhibit a comparable performance when the solution of the waveguide problem is a plane wave (see Eq. (29)). Consequently, we present here a comparison between the

Table 4: Sensitivity of the total relative error and of the number of dofs to the mesh refinement for SDGM equipped successively with R-7-2 and R-11-3, and for $ka = 20$.

# elements per wavelength	Total relative error		# dofs	
	R-7-2	R-11-3	R-7-2	R-11-3
3	7%	0.04%	720	1,080
6	0.4%	0.002%	3,040	4,560
9	0.1%	0.0002%	6,960	10,440
12	0.04%	0.0001%	12,480	18,720

two methods in the case where the exact solution is not a plane wave. We consider the case where the exact solution is given by $u(x,y) = e^{ikxy}$. We set
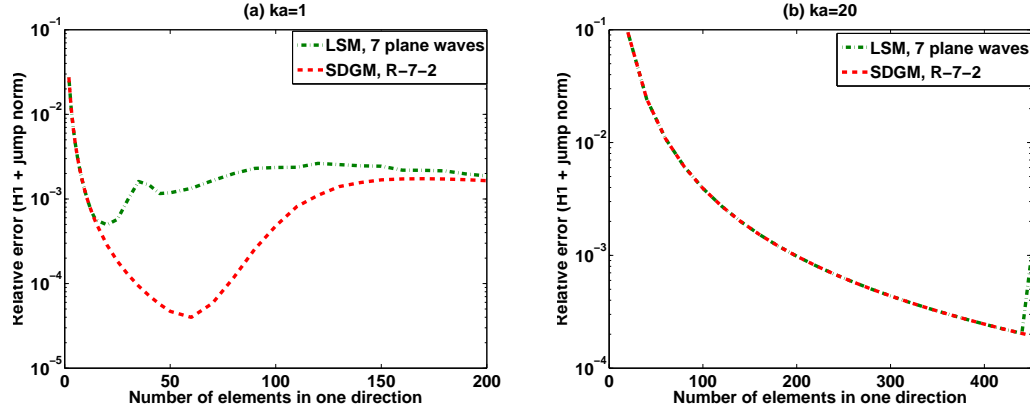
Figure 6: Sensitivity of the total relative error to the mesh refinement: Comparison between SDGM equipped with R-7-2 and LSM equipped with 7 plane waves, and for $ka = 1$ (left) and $ka = 20$ (right).

$ka = 1$ and 20, and we vary the mesh. The results are reported in Fig. 6. These results suggest that for $ka = 1$ (see Fig. 6(a)) SDGM is slightly superior to LSM in terms of accuracy. For $ka = 20$ (see Fig. 6(b)), both methods deliver the same level of accuracy. Note however that in the case of LSM, there is a jump of about one order of magnitude in the relative error in the region corresponding to about 130 elements per wavelength. We could not discretize more to investigate thoroughly, due to the limitation of our computing platform. This result tends to indicate that even for problems that admit solutions that are not plane waves, both methods deliver solutions with comparable level of accuracy.

5.1.2 High-frequency regime

We present the results of three sets of experiments in which the exact solution is a plane wave (see Eq. (29)). The first experiment compares the accuracy of SDGM equipped successively with R-7-2 and R-11-3 for three values of ka: 50, 100, 200, and for a fixed resolution: $kh = 2$, corresponding to about 3 elements per wavelength. The relative errors obtained for each propagation angle are depicted in Fig. 7. We also report in Table 5 the values of the total relative errors. These results show, as expected, that SDGM equipped with R-11-3 leads to a better accuracy level than with R-7-2. Note that there is an improvement of the accuracy ranging from two to three orders of magnitude depending on the frequency regime. Moreover, this significant improvement in the accuracy level requires an increase in the computational cost by only 50% (see Table 4). Observe the impressive result obtained for $ka = 200$ for which, using only about 3 elements per wavelength, SDGM delivers a solution with an accuracy level of about 0.2%.

Note that SDGM equipped with R-11-3 remains superior to DGM equipped with R-11-3 in this range of frequency regime, as illustrated in Fig. 8 for $ka = 200$
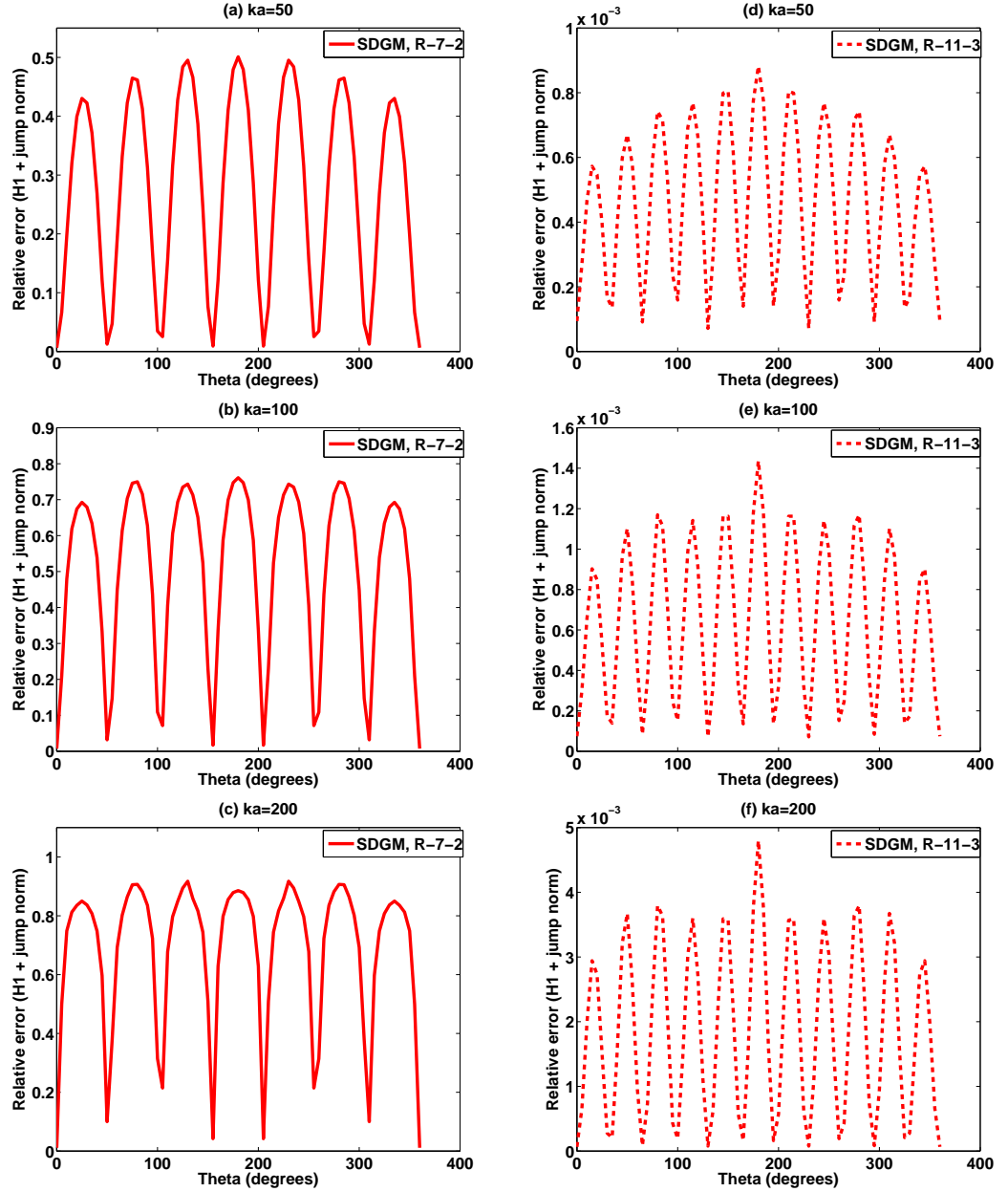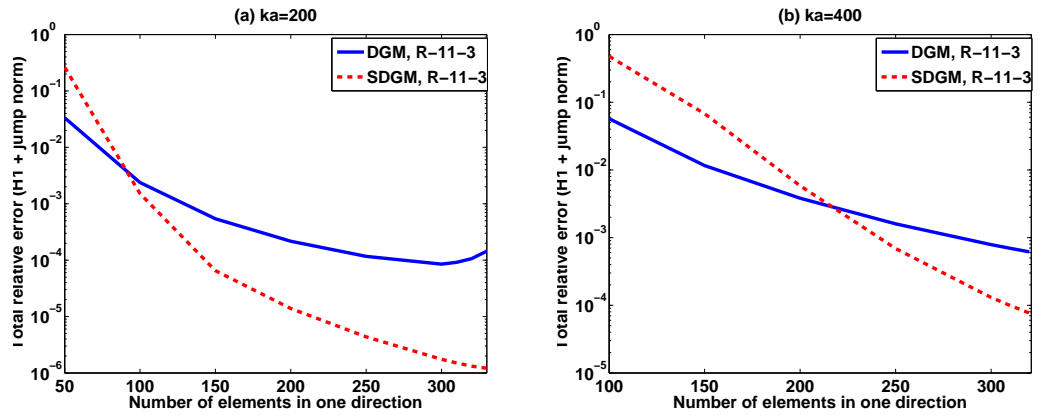
Figure 7: Performance comparison between SDGM equipped with R-7-2 (left) and R-11-3 (right), for a fixed resolution $kh = 2$.

Table 5: Sensitivity of the total relative error to the frequency: Comparison between SDGM equipped successively with R-7-2 and R-11-3, and for $kh = 2$.

ka	R-7-2	R-11-3
50	28%	0.05%
100	51%	0.07%
200	69%	0.2%

Figure 8: Sensitivity of the total relative error to the mesh refinement: Comparison between SDGM and DGM equipped with R-11-3, for $ka = 200$ (left) and $ka = 400$ (right).

and 400.

Next, we compare the computational cost for two elements R-11-3 and R-13-4 to achieve a prescribed level of accuracy. Note that the R-13-4 element was introduced in [11] and corresponds to $n^K = 13$ in Eq. (27) and four dofs for the Lagrange multipliers given by:

$$\lambda_h = \mu_1 e^{\mathrm{i}\,ks} + \mu_2 e^{-\mathrm{i}\,ks} + \mu_3 e^{\mathrm{i}\,k\frac{\sqrt{2}}{2}s} + \mu_4 e^{-\mathrm{i}\,k\frac{\sqrt{2}}{2}s}. \qquad (32)$$

We perform this numerical experiment for two frequency values, $ka = 200$ and 400, and we fix the level of accuracy to 10%, 5% and 1%. The obtained results are reported in Table 6. These results suggest the following:

- SDGM is clearly efficient in the high-frequency regime. Indeed, using about three elements per wavelength only is sufficient to reach an accuracy level of 1% with R-11-3 and R-13-4 elements for both frequency values $ka = 200$ and 400.

- These results clearly suggest that in high-frequency regime, it is preferable to use higher-order elements rather than refining the mesh to maintain the same accuracy level. For example, in order to reach 1% on the relative

Table 6: Mesh resolution and number of dofs for SDGM equipped successively with R-11-3 and R-13-4 for three fixed levels of accuracy, and for ka=200 and ka=400.

(a) $ka = 200$

Level of accuracy	# elements per wavelength		# dofs	
	R-11-3	R-13-4	R-11-3	R-13-4
10%	1.88	1.32	$42,480$	$27,552$
5%	2.10	1.44	$53,064$	$33,120$
1%	2.51	1.73	$75,840$	$47,520$

(b) $ka = 400$

Level of accuracy	# elements per wavelength		# dofs	
	R-11-3	R-13-4	R-11-3	R-13-4
10%	1.88	1.48	$171,360$	$139,872$
5%	2.46	1.60	$293,904$	$164,832$
1%	2.95	1.99	$421,872$	$256,032$

error, SDGM equipped with R-11-3 requires 50% more dofs than R-13-4 for both $ka = 200$ and 400. This means that the computational cost is reduced by more than 30% when using R-13-4 instead of R-11-3 for reaching a fixed 1% level of accuracy.

5.2   Unstructured mesh

We present in this section numerical results to illustrate the effect of the mesh distortion on the performance of SDGM. The results presented here are obtained in the case where the exact solution of BVP is a plane wave given by Eq. (29). We have used the technique described in [8] to generate distorted meshes from a uniform mesh in order to compare the performance of SDGM to DGM. More specifically, we have displaced each node of a uniform mesh by a random vector, multiplied by a scaling factor, δ in $[0, 0.5]$ chosen to avoid interpenetration of the elements. We have performed numerical experiments in the case of five meshes corresponding to $\delta = 0$, 0.1, 0.3, 0.4 and 0.45 (see Fig. 9). Note that $\delta = 0$ corresponds to a uniform mesh, whereas $\delta = 0.45$ corresponds to the most unstructured mesh considered in this series of experiments. Similarly to the experiments presented in [8], we have fixed $ka = 30$ and a propagation angle $\theta = 67.5°$. Recall that the relative error for both methods reaches its highest value for this propagation angle. The results obtained in Fig. (10) clearly indicate that there is a "little" effect of the mesh distortion on the accuracy delivered by SDGM. Moreover, the comparison with DGM equipped with R-8-2 (recommended by the authors of DGM for $ka = 30$ [8]) shows, as expected, that SDGM is clearly superior in terms of stability and accuracy.
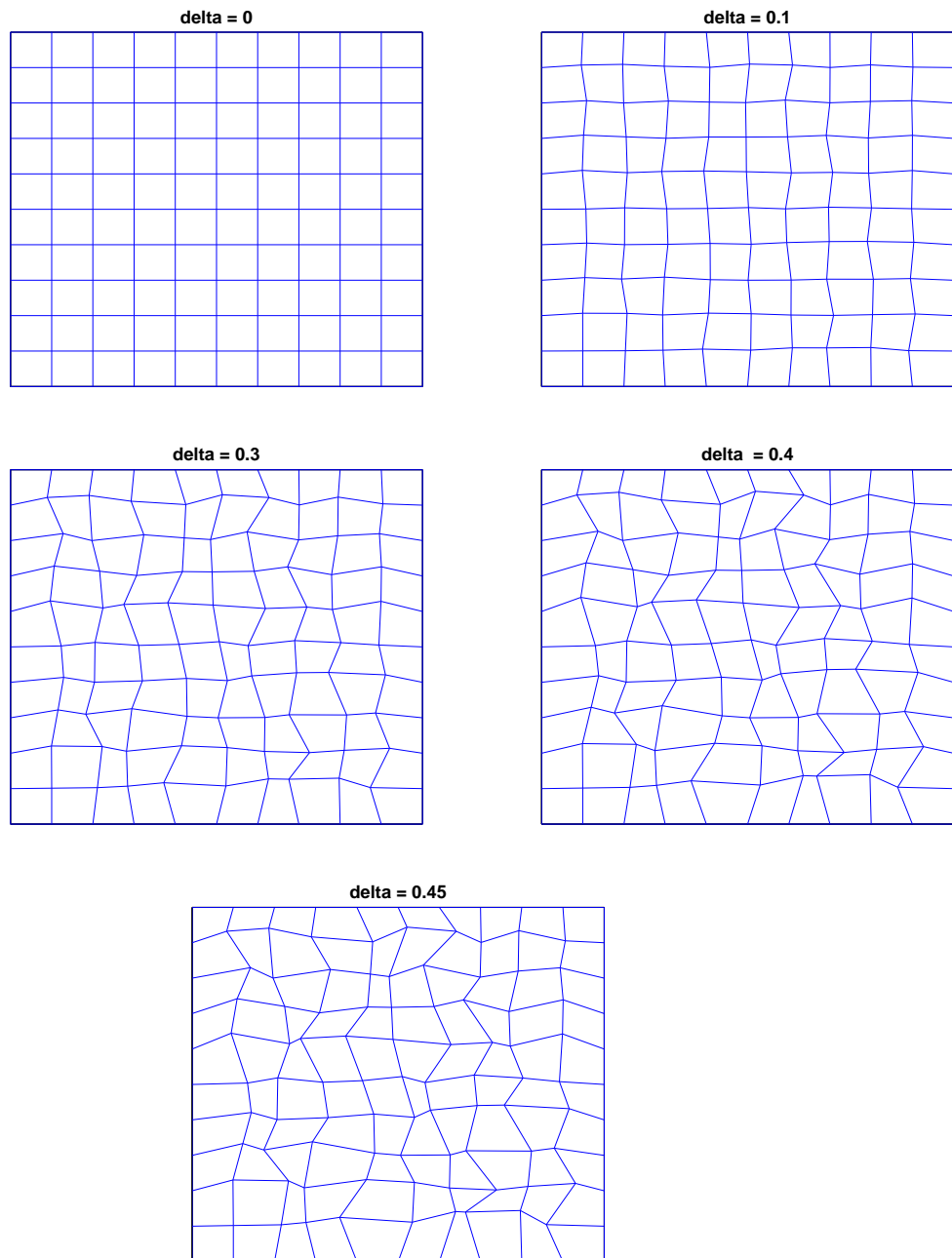
Figure 9: A class of unstructured meshes used for analyzing the effect of the mesh distortion on the performance of SDGM.
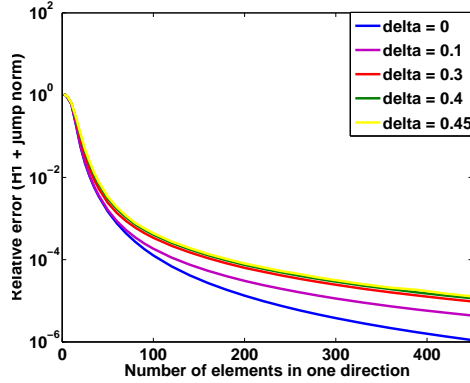
Figure 10: Sensitivity of the relative error to the mesh refinement in the case of SDGM equipped with Q-7-2 for different unstructured meshes when $ka = 30$ and $\theta = 67.5°$

6   Conclusion and perspectives

We have designed a DG-type method, called SDGM, for solving Helmholtz problems. The method can be viewed as being "between" the DGM formulation designed by Farhat *et al* in [7, 8, 9] and the LSM formulation suggested by Monk-Wang in [17]. The numerical results obtained in the case of waveguide problems are very promising. They show that the proposed method is stable and accurate. For example, for the R-7-2 element, SDGM remains stable for a mesh resolution with over 1000 elements per wavelength. Moreover, in the high frequency regime SDGM delivers results with high level of accuracy. For instance, when $ka = 400$ and using only about 3 elements per wavelength, SDGM equipped with R-11-3 delivers a solution with an accuracy level of 0.6% on the relative error. We have also observed that in high-frequency regime it is preferable to increase the order of the element rather than refining the mesh for reaching a good level of accuracy. For example, for $ka = 400$ and for an accuracy equal to 1% on the relative error, the R-13-4 element reduces the number of dofs with up to 40% when compared to the R-11-3 element.

The comparison with DGM reveals that SDGM is clearly more robust than DGM in terms of accuracy and stability. On the other hand, the method delivers results comparable to LSM. However, we have observed that for problems whose solutions are not plane waves, SDGM has the potential to be more efficient. It might be the case for two- and three-dimensional acoustic scattering problems in which the scattered field is not a plane wave. We are currently conducting such an investigation.

References

[1] M. Amara, H. Calandra, R. Djellouli, M. Grigoroscuta-Strugaru, A modified discontinuous Galerkin method for Helmholtz prob-
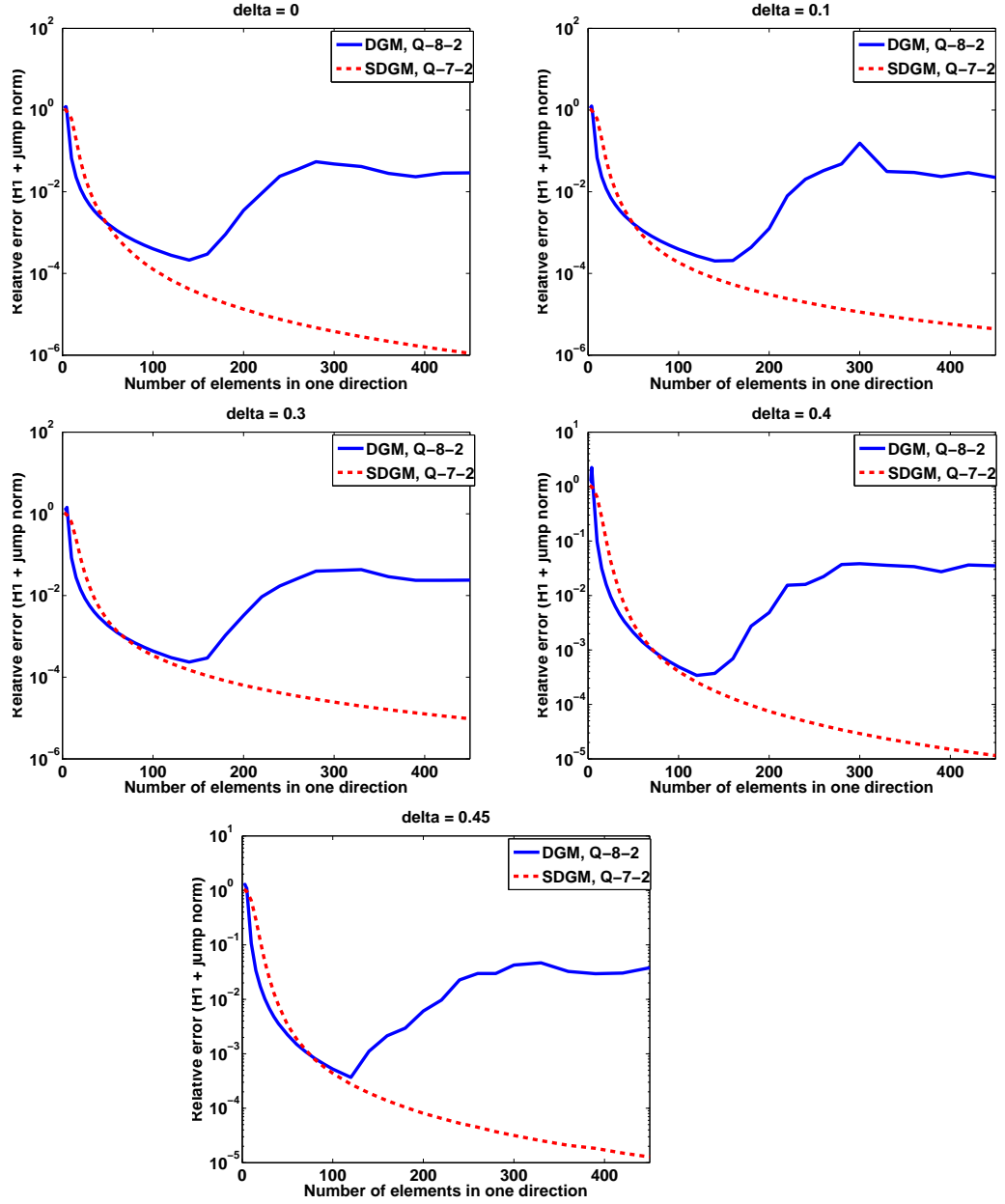
Figure 11: Sensitivity of the relative error to the mesh refinement in the case of SDGM equipped with Q-7-2 and DGM equipped with Q-8-2 for different distorted meshes, and for $ka = 30$ and $\theta = 67.5°$.

lems, Technical Report INRIA No. 7050 (2009) available online at `http://hal.archives-ouvertes.fr/inria-00421584/fr/`.

[2] M. Amara, R. Djellouli, C. Farhat, Convergence analysis of a discontinuous Galerkin method with plane waves and Lagrange multipliers for the solution of Helmholtz problems, SIAM J. Numer. Anal. 47 (2009) 1038-1066.

[3] I. Babuška, I.J.M. Melenk, The partition of unity method, Internat. J. Numer. Methods Eng. 40 (1997) 727-758.

[4] I. Babuška, S. Sauter, Is the Pollution Effect of the FEM Avoidable for the Helmholtz Equation Considering High Wave Numbers?, SIAM J. Numer. Anal. 34 (1997) 2392-2423.

[5] O. Cessenat, B. Després, Application of an ultra-weak variational formulation of elliptic PDEs to the two-dimensional Helmholtz problems, SIAM J. Numer. Anal. 35 (1998) 255-299.

[6] W. Desmet, P. van Hal, P. Sas, D. Vandepitte, A computationally efficient prediction technique for the steady-state dynamic analysis of coupled vibro-acoustic systems, Advances in Engineering Software 33 (2002) 527-540.

[7] C. Farhat, I. Harari, U. Hetmaniuk, A discontinuous Galerkin method with Lagrange multipliers for the solution of Helmholtz problems in the mid-frequency regime, Comput. Methods Appli. Mech. Eng. 192 (2003) 1389-1419.

[8] C. Farhat, P. Wiedemann-Goiran, R. Tezaur, A discontinuous Galerkin method with plane waves and Lagrange multipliers for the solution of short wave exterior Helmholtz problems on unstructured meshes, Wave Motion 39 (2004) 307-317.

[9] C. Farhat, R. Tezaur, P. Wiedemann-Goiran, Higher-order extensions of a discontinuous Galerkin method for mid-frequency Helmholtz problems, Internat. J. Numer. Methods Eng. 61 (2004) 1938-1956.

[10] B. V. Genechten, B. Bergen, D. Vanderpitte, W. Desmet, A Trefftz-based numerical modeling framework for Helmholtz problems with complex multiple-scatterer configurations, J. Comput. Phys. 229 (2010) 6623-6643.

[11] M. Grigoroscuta-Strugaru, Contribution à la résolution numérique des problèmes de Helmholtz, University of Pau, France, December 2009, available online at `http://tel.archives-ouvertes.fr/`.

[12] P. Grisvard, Elliptic Problems in Non Smooth Domains Pitman, Boston, 1985.

[13] J. Hadamard, Lectures on Cauchy's Problem in Linear Partial Differential Equations, Yale University Press, New Haven, 1923.

[14] L. Hörmander, The Analysis of Linear Partial Differential Operator, Springer-Verlag, New York, 1985.

[15] G. Karypis, V. Kumar, A fast and high quality multilevel scheme for partitioning irregular graph, SIAM Journal on Scientific Computing 20 (1998) 359-392.

[16] F. Magoulès, Computational Methods for Acoustics Problems, Saxe-Coburg Publications, 2008.

[17] P. Monk, D.Q. Wang, A least-squares method for the Helmholtz equation, Comput. Methods Appli. Mech. Eng. 175 (1999) 411-454.

[18] M.E. Rose, Weak element approximations to elliptic differential equations, Numer. Math. 24 (1975) 185-204.

[19] O. Schenk, K. Gärtner, Solving unsymmetric sparse systems of linear equations with PARDISO, Journal of Future Generation Computer Systems 20 (2004) 475-487.

[20] O. Schenk, K. Gärtner, On fast factorization pivoting methods for symmetric indefinite systems, Elec. Trans. Numer. Anal. 23 (2006) 158-179.

[21] M.E. Taylor, Partial Differential Equations I: Basic Theory, Springer-Verlag, New York, 1997.

[22] R. Tezaur, A. Macedo, C. Farhat, R. Djellouli, Three-dimensional finite element calculations in acoustic scattering using arbitrarily shaped convex artificial boundaries, Internat. J. Numer. Methods Eng. 53 (2002) 1461-1476.

Contents